Axisymmetric Adhesive Contact under Equibiaxial Stretching

Julie F. Waters, Jonathan Kalow, Huajian Gao, Pradeep R. Guduru*
School of Engineering, Brown University, RI 02912, USA
*Corresponding author. Email: Pradeep_Guduru@Brown.edu, Tel: 401 863 3362

Abstract

This paper experimentally examines axisymmetric adhesive contact under equi-biaxial stretch of the substrate. It is motivated by recent theoretical models which predict that the contact radius decreases sharply beyond a critical strain, with an instability that can result in spontaneous detachment or gross slipping across the contact area. The model system in the present experiments consists of convex glass lenses resting on PDMS sheets, which are subjected to equi-biaxial stretch in a specially designed experimental setup. It is shown that the evolution of the contact area is well described by the theoretical model after accounting for the mode-mixity dependence of work of adhesion at the contact edge. More significantly, the conditions of instability observed in the experiments were well predicted by the model. The findings are expected to be significant in predicting soft material contact behavior, such as that in biological adhesion.

Keywords: Adhesion; biaxial stretch; contact mechanics; instability; mixed-mode fracture.

1. Introduction

It has been widely reported that living cells respond to substrate strain by re-orienting themselves away from the direction of the stretch [1-12]. It has also been reported that the extent of re-orientation depends on the strain amplitude [8-9]. Motivated by such observations, Chen and Gao [13-16] developed contact models for how symmetric contact between two elastic solids evolves under substrate strain. In particular, they considered the contact between a cylinder and a half-space under uniaxial strain [13], and that between a sphere and a half-space under equi-biaxial strain [14]. The canonical result that they demonstrated is the following; in the absence of any normal force, the contact radius decreases with substrate strain and approaches zero continuously. In the presence of a normal force, as the substrate strain increases, the contact area decreases until a critical value, beyond which it becomes unstable and spontaneous detachment is predicted. The importance of the contact problem under substrate straining extends beyond the behavior of cells; it can be a spontaneous detachment mechanism in biological attachment systems, which involve soft materials [17-26]. The objective of this article is to carry out an experimental investigation of adhesive contact under substrate strain, compare the results with those of Chen and Gao model prediction and suggest any improvements to the model if necessary. In the next section, a revised form of the Chen and Gao [14] model is presented, in which the effect of mode-mixity on work of adhesion is considered phenomenologically. The results are used to motivate the subsequent experimental section.

2. Axisymmetric adhesive contact under equi-biaxial straining

Consider a sphere of radius R in no-slip contact with a half-space, which is subsequently subjected to an equi-biaxial strain of ε_m, as illustrated in Fig. 1. A circular contact area of radius a is established in the presence of a compressive normal force of P. Although Chen and Gao [14] developed a general solution for two elastic spheres in contact, here we will consider its limiting case of a rigid sphere in contact with an incompressible elastic half-space, which approximates

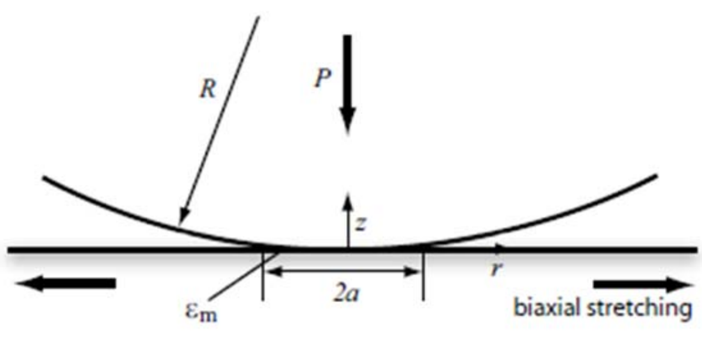

Figure 1: Schematic illustration of the geometry of the biaxial stretching contact problem. A rigid sphere of radius R is initially in no-slip contact with a half-space under external normal loading P. Biaxial stretching induces a mismatch strain ε_m within the contact radius a.

the experiments involving glass spheres in contact with elastomeric substrates. The stress intensity factors at the contact periphery for this case are given by

$$K_I = \frac{2E^* a^{3/2}}{3\sqrt{\pi}R} - \frac{P}{3\sqrt{\pi}a^{3/2}} \tag{1}$$

and

$$K_{II} = -2E^* \varepsilon_m \sqrt{\frac{a}{\pi}} \tag{2}$$

where, $E^* = E/(1 - \nu^2)$ is the reduced elastic modulus, R is the radius of the sphere, a is the radius of contact, and P is the applied load ($P > 0$ for compression). For this specific case, the stress intensity factors are decoupled; K_I is dependent upon P only, while K_{II} is dependent upon the mismatch strain ε_m only. To incorporate the phenomenological mixed-mode fracture criterion, the energy release rate G is set equal to a mode-mixity-dependent work of adhesion $w(\psi)$:

$$G = \frac{K_I^2 + K_{II}^2}{2E^*} = w(\psi) \tag{3}$$

where the phase angle ψ was defined as $\tan^{-1}(K_{II}/K_I)$. The parameterization of Hutchinson and Suo [27] is chosen to describe $w(\psi)$ as follows,

$$w(\psi) = w_0 \xi(\psi) = w_0\left(1 + \tan^2\left[(1-\lambda)\psi\right]\right) \tag{4}$$

where w_0 is the work of adhesion for pure mode I loading. The parameter λ in Eq. 4 determines the influence of mode mixity and is bounded between 0 and 1. Figure 2 shows the variation of w/w_0 with ψ for a range of λ. If $\lambda = 1$, $\xi(\psi) = 1$ and $w(\psi) = w_0$ for all ψ, which is the classical surface energy criterion used by Chen and Gao [14]. If $\lambda = 0$, the crack is "fully shielded" from any effects of mode II and crack advance depends only upon the mode I component. The $\lambda = 0$ case is thus often referred to as being "K_{II}–independent".

Using Eqs. (1)–(2) and Eq. (4), the contact equilibrium condition given by Eq. (3) can be expressed as

$$a^3 + 9R^2\varepsilon_m^2 a - \frac{9\pi w_0 \xi(\psi) R^2}{2E^*} + \frac{9R^2P^2}{16E^* a^3} - \frac{3PR}{2E^*} = 0 \tag{5}$$

which determines the relationship between a and ε_m for a given w_0, $\xi(\psi)$, R, and P. Chen and Gao [14] found that, when $w = w_0$, this contact problem could be described by the dimensionless parameters

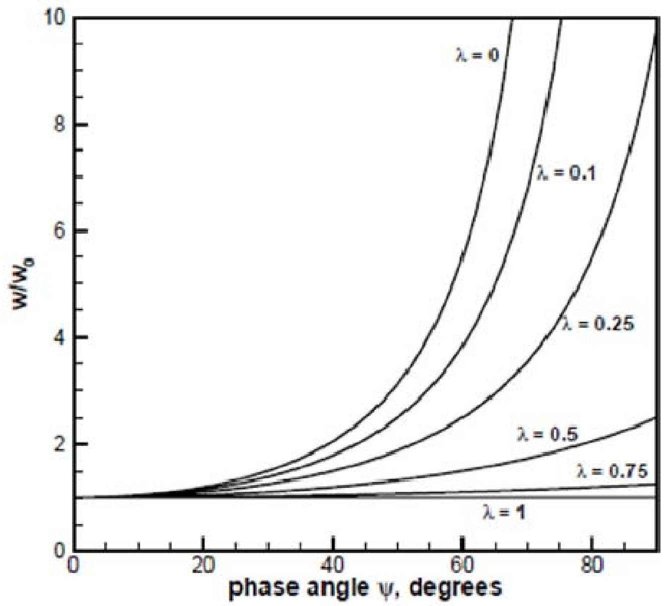

Figure 2: Phenomenological model for the effective work of adhesion w increasing with phase angle of mode mixity ψ. $\lambda = 1$ corresponds to w remaining constant, similar to "ideally brittle" fracture, while $\lambda = 0$ corresponds to a "fully shielded" case.

$$\hat{a} = \frac{a}{a_0}, \qquad \hat{R} = \frac{R}{a_0}, \qquad \hat{F} = -\frac{3PR}{4E^* a_0^3} \tag{6}$$

where a_0 is the contact radius at $\varepsilon_m = 0$ with $w = w_0$, equivalent to that for the classical JKR case. In the present case, with $w = w_0\, \xi(\psi)$ as defined in Eq. (4), Eq. (5) can be normalized as

$$\hat{a}^3 + 9\hat{R}^2\varepsilon_m^2\hat{a} + \hat{F}\hat{a}^{-3} - \xi(\psi)\left(1 + \hat{F}/2 + \hat{F}^2\right) + \hat{F}/2 = 0 \tag{7}$$

where the phase angle ψ can be expressed in terms of the dimensionless parameters as

$$\psi = \tan^{-1}\left(\frac{-3\hat{R}\varepsilon_m}{\hat{a} + \hat{F}\hat{a}^{-2}}\right) \tag{8}$$

Using this expression, Eq. (7) can be solved numerically for ε_m for given values of $\hat{a}$, $\hat{R}$, and $\hat{F}$. Sample results are shown in Fig. 3. Increasing ε_m is seen to reduce the contact area from its initial value of a_0, similar to the reduction in contact area seen for increased tangential loading in the case studied by Waters and Guduru [28,29], where an adhesive contact was subjected to normal and tangential loads. Of note is that, qualitative differences in behavior are predicted here for neutral and finite normal loading. For the case of neutral loading ($\hat{F}$ = 0) shown in Fig. 3a, there is a smooth transition towards a/a_0 = 0 for increasing strain. However, for the case of compressive loading ($\hat{F}$ = −0.025) shown in Fig. 3b, an instability is seen; there is a critical value of ε_m beyond which higher mismatch strains cannot be sustained by the interface. Such instabilities are seen for any finite compressive or tensile normal loading. In the tensile case, the instability initiates spontaneous separation at a critical value of mismatch strain; in the compressive case, reaching a critical value of mismatch strain triggers a slip event followed by reattachment. In both cases, the effect of decreasing λ (i.e., increasing the amount of dissipation) in the expression for $w(\psi)$ is to increase the critical mismatch strain at which such instabilities occur.

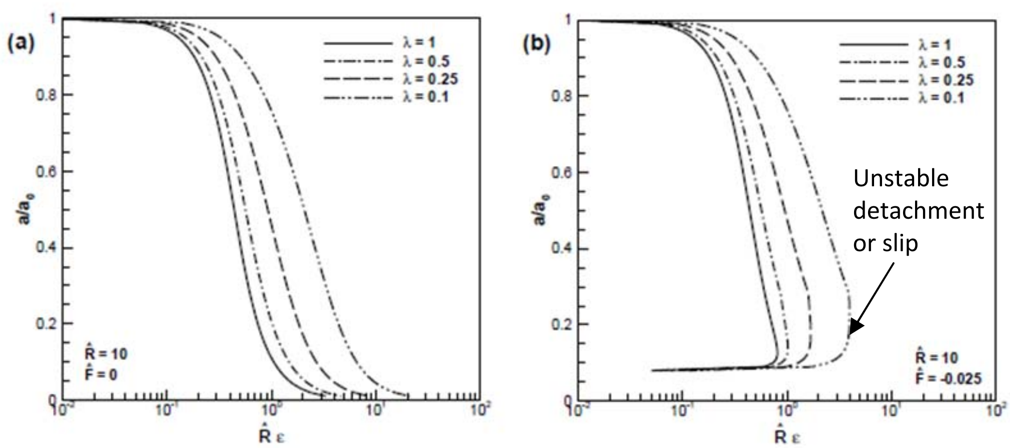

Figure 3: Theoretical predictions for the reduction in contact radius a/a_0 versus normalized mismatch strain $\hat{R}\varepsilon_m$. (a) When normalized load $\hat{F} = 0$, a smooth transition to zero contact area is predicted. (b) Under a compressive load $\hat{F} = -0.025$, an instability is seen; there is a critical value of ε_m beyond which higher mismatch strains cannot be sustained by the interface without slip occurring. Qualitatively similar instabilities are also seen for tensile normal loading. Note that in (b) the location of instability is shown for l = 0.1 case only. Each of the other curves has an instability where the tangent to the curve is vertical.

3. Biaxial stretching experiments

The influence of equi-biaxial strain on adhesive contact was investigated through a series of experiments, in which PDMS (polydimethilsiloxane) sheets were used as substrates subjected to strain. Spherical convex glass lenses of various radii were brought into contact with PDMS sheets, and the contact area between the lens and the PDMS substrate was observed and recorded as strain was applied at a controlled rate, as described below. The choice of the model experimental configuration is guided by the existing body of literature that examined other aspects of adhesion between glass lenses and PDMS substrates [30].

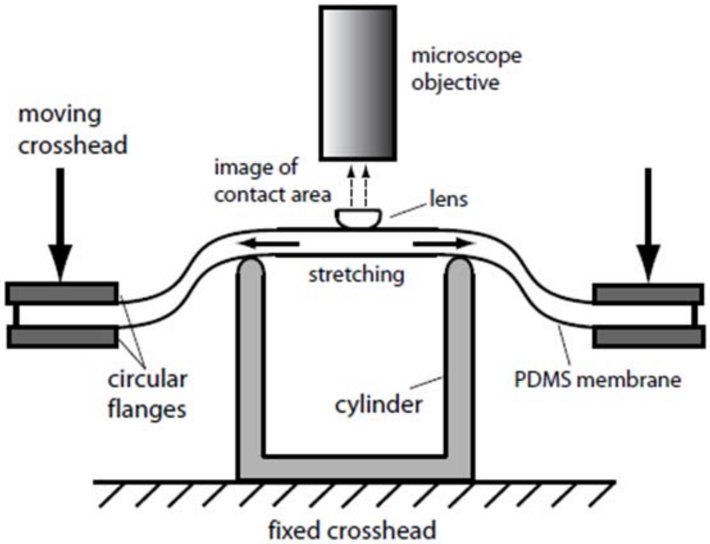

Figure 4: Schematic diagram of biaxial stretching experiment. Circular flanges are used to secure a PDMS membrane to the moving crosshead of an Instron machine. The motion of the crosshead stretches the PDMS over an aluminum cylinder. A spherical convex lens is placed on the surface in the center of the membrane to idealize the biaxial strain condition. The weight of the lens provides a constant compressive normal load *P*. Images of the contact area are observed and recorded during the experiment using a microscope objective attached to a digital camera.

PDMS (Sylgard 184, Dow Corning) samples were prepared by casting on a smooth 115 mm diameter borosilicate glass plates, resulting in circular PDMS sheets, approximately 4 mm in thickness. The elastomer base and curing agent were mixed in a 10:1 ratio by weight and degassed in a vacuum chamber for 1 hour. The mixture was cured in an oven at 75^{o}C for 3 hours. The reduced elastic modulus for these samples was measured to be 2.3 MPa, as described in Waters and Guduru [28,29]. The samples were gently dusted with spray paint in order to introduce particles on the surface which would be used to measure strain. A circular area of 2-3 mm diameter at the center of the sample was protected from the spray paint, where the glass lenses would be brought into contact. The PDMS surface cast against the glass plate was used for all experiments, in order to minimize roughness, defects and curvature.

R (mm)	mass (mg)	P (mN)	w_0 (mJ/m^2)	$\hat{R}$	$\hat{F}$
2.55	13.5	0.13	53	19	-0.05
2.55	13.5	0.13	40	21	-0.06
4.25	15.1	0.15	62	22	-0.03
6.2	17.8	0.17	70	24	-0.02

Table 1: Parameters for the biaxial stretching experiments.

The experimental setup to equi-biaxially stretch PDMS sheets is illustrated in Fig. 4. PDMS sheets were clamped flat between a pair of aluminum flanges and lowered concentrically over a stationary aluminum cylinder, in a manner similar to stretching the head of a drum over its body. The cylinder was rigidly attached to the lower crosshead of an Instron 5880 materials testing machine, while the flanges holding the PDMS were rigidly attached to the upper crosshead through a 50 kN load cell. Each flange had a 76 mm diameter hole in the center over which the 115 mm PDMS disc was placed. Each flange had a pair of 2.5 mm thick and 1.3 mm tall concentric ridges to prevent the clamped sheet from slipping in the grip during loading. The inner and outer diameters of the aluminum cylinder were 32 mm and 38 mm respectively. The top edge of the cylinder in contact with the PDMS sheet had radius of 1.5 mm; it was polished smooth to allow the PDMS sheet to slide on it with minimal friction. In addition, Dupont Krylox lubricant (Duport Corporation) was applied on the cylinder surface.

Convex glass lenses (CVI Corporation, Rochester, NY) with radius of curvature R were gently placed at the center of the unstretched PDMS surface as illustrated in Fig. 4; the central location prevents unwanted lateral movement of the lens in the field of view of the microscope during the experiment. Note that the weight of the lens provides a constant compressive normal load P on the contact area. The contact area was imaged with a microscope (2.5× objective) placed directly above the center of the PDMS sheet and the images were acquired with a digital

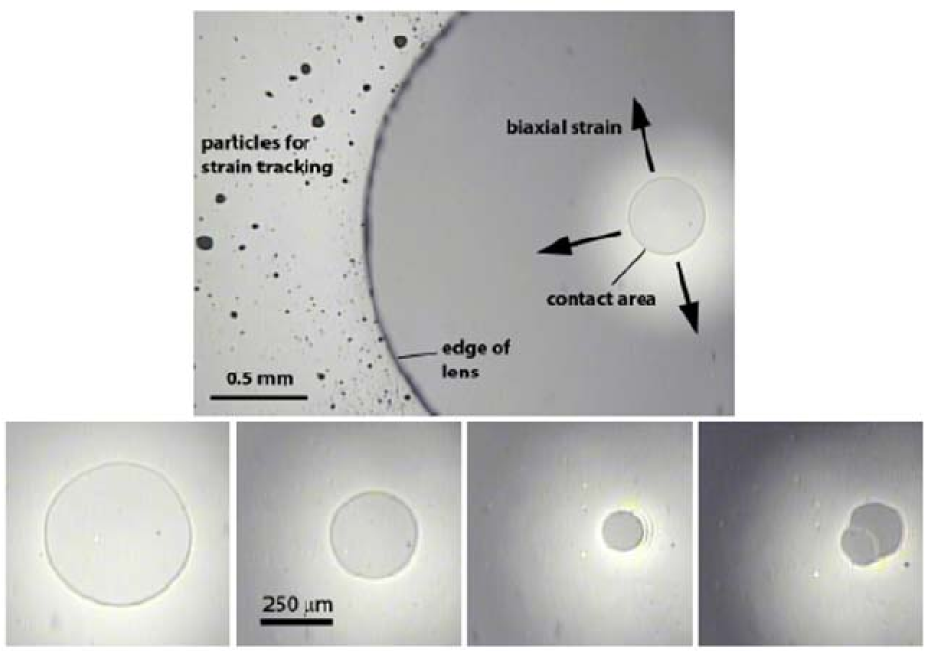

Figure 5: Representative images of contact area during the biaxial stretching experiments (R = 6.2 mm). Top: Full field of view. Spray paint particles outside the area of contact were used for strain measurement. Bottom: Series of images illustrates shrinking contact area with increased stretching. Final image shows reattachment after slip instability.

camera attached to the microscope. During the experiments, the PDMS sheet was lowered onto the cylindrical ring at a speed of 6 mm/min; displacement and load data were collected at a rate of 1 Hz. The substrate strain was measured from the microscope images, by tracking the distance between pairs of paint particles. Figure 5 shows a typical sequence of images recorded during the experiment. The top image illustrates the field of view during the experiment, which contains the contact area as well as the paint particles. The sequence of images at the bottom shows the shrinking contact area with increasing strain. The last frame illustrates reattachment over a larger contact area following a slip instability.

In order to compare the experimental results to the theoretical model, the initial contact area a_0 was used to determine the mode I work of adhesion w_0 using the JKR theory [31] equation

$$w = \frac{1}{8\pi E^* a^3}\left(\frac{4E^* a^3}{3R} - P\right)^2 \tag{9}$$

The parameters $\hat{R}$ and $\hat{F}$ were then computed, as defined in Eq. 6. This data is summarized in Table 1. Figure 5 compares the experimental data to the theoretical results. It was found that the theoretical curves for this range of parameters were virtually identical on a logarithmic scale;

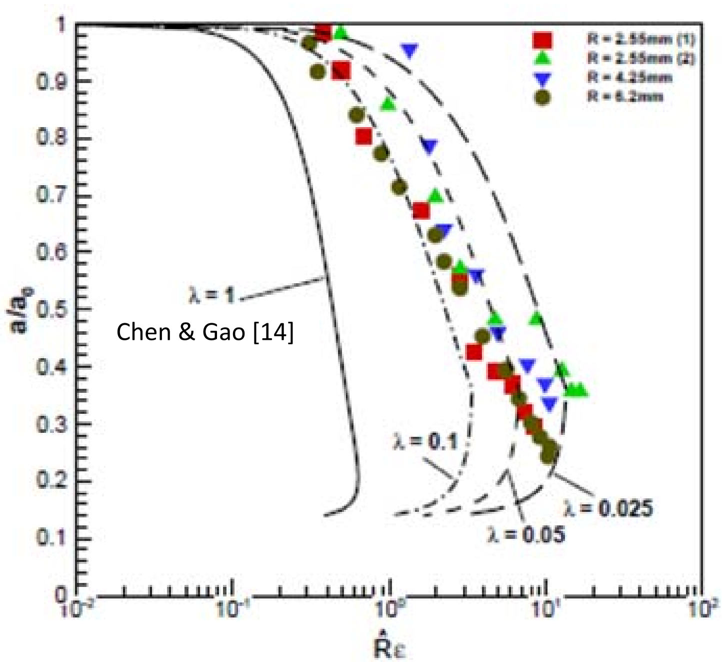

Figure 5: Results of the biaxial stretching experiment. Fitting of the phenomenological mixed mode contact model with $\lambda \sim 0.05 - 0.1$ provides a better fit to the data than the model of Chen and Gao [14] ($\lambda = 1$). The critical mismatch strain and contact radius at the onset of slip instability are also captured well by the phenomenological model.

thus, only the curves for $\hat{F} = -0.05$ and $\hat{R} = 19$ are shown. Fig. 5 shows that the Chen and Gao [14] model ($\lambda = 1$) significantly underpredicts the contact radius a/a_0 for a given mismatch strain ε_m. Considering the mixed mode fracture criterion (Eqs. 3 & 4) and adding dissipation by decreasing λ gives a much better agreement with the experimental results, with $\lambda = 0.05 - 0.1$ giving a reasonable match. The small value of λ indicates that substantial dissipation occurs in the interface, which is similar to the observation of Liechti and Chai [32] in the context of mixed mode interfacial fracture mechanics. More significantly, the experiments capture the instability predicted by the theoretical model at a critical value of $\varepsilon_{\mathrm{m}} \sim 0.53$ (or $\hat{R}\varepsilon_m \sim 10$). The data points plotted in Fig. 5 are those prior to the onset of the instability, and the values of a/a_0 and ε_m at which the instability occurs in the experiments is estimated well by the model. Beyond this point of instability, the contact area spontaneously slips and increases in size due to reattachment. It also loses its symmetrical shape possibly because the interface does not slip symmetrically; it initiates at a point on the periphery and spreads across, while reattaching simultaneously in the slip zone. The instability indicates that slip is not a gradual process as seen in Hertzian contact models, but rather that the no-slip condition provides an accurate description of the adhesive contact of PDMS under these loading conditions. These results from biaxially strained contact experiments, with symmetric circular contact areas throughout the tests, validate that the model developed using the higher precision data of the initial symmetric peeling stage of tangential loading as reported by Waters and Guduru [28, 29], and has general utility for a range of contact problems. Use of a mode-mixity-dependent work of adhesion provides for better agreement with experimental data and will allow for more accurate predictions of contact problems involving soft materials.

4. Summary

The mechanics of adhesive contact under biaxial straining of the substrate is an important problem in contact problems involving soft materials, such as those that appear in cell-substrate interaction and reversible attachment-detachment of biological organisms. A theoretical model developed by Chen and Gao [14] showed that the contact area decreases precipitously when the biaxial strain exceeds a critical value; subsequent increase in strain can result in an instability that appears as either spontaneous detachment or interfacial slip. An experimental investigation has been carried out here to study adhesive contacts under biaxial strain and examine the predictions of Chen and Gao [14] model. The main result is that the experiments show contact instability, as predicted by the model. Further, the evolution of contact area with strain is well predicted by the model, after the fracture criterion is modified to account for additional dissipation due to mixed mode conditions at the contact periphery. A phenomenological mixed mode work of adhesion, similar to that of Hutchinson and Suo [27] yielded good agreement between the experiment and model predictions, with $\lambda = 0.05 - 0.1$, suggesting significant dissipation due to mode mixity.

Acknowledgements

This work was supported by the Mechanics of Multifunctional Materials and Microsystems program of the Air Force Office of Scientific Research (grant no. FA9550-05-1-0210; program manager, Dr Les Lee) and the National Science Foundation (grant no. CMS-0547032).

References

1. Galbraith, C.G., Sheetz, M., 1998. Forces on adhesive contacts affect cell function. Curr. Opin. Cell Biol. 10, 566–571.

2. Huang, S., Ingber, D.E., 1999. The structural and mechanical complexity of cell-growth control. Nat. Cell. Boil. 1, E131–E138.

3. Geiger, B., Bershadsky, A., 2002. Exploring the neighborhood: adhesion-coupled cell mechanosensors. Cell 110, 139–142.

4. Haston, W.S., Shields, J.M., Wilkinson, P.C., 1983. The orientation of fibroblasts and neutrophils on elastic substrata. Exp. Cell Res. 146, 117–126.

5. Dartsch, P.C., Hammerle, H., 1986. Orientation response of arterial smooth muscle cells to mechanical stimulation. Eur. J. Cell Biol. 41, 339–346.

6. Dartsch, P.C., Betz, E., 1989. Response of cultured endothelial cells to mechanical stimulation. Basic Res. Cardiol. 84, 268–281.

7. Iba, T., Sumpio, B.E., 1991. Morphological response of human endothelial cells subjected to cyclic strain in vitro. Microvasc. Res. 42, 245–254.

8. Wang, H.C., Wallace, I., Raymond, B., Edward, S.G., 1995. Cell orientation response to cyclically deformed substrates: experimental validation of a cell model. J. Biomech. 28, 1543–1552.

9. Takemasa, T., Sugimoto, K., Yamashita, K., 1997. Amplitude-dependent stress fiber reorientation in early response to cyclic strain. Exper. Cell Res. 230, 407–410.

10. Bischofs, I.B., Schwarz, U.S., 2003. Cell organizing in soft media due to active mechanosensing. Proc. Natl. Acad. Sci. USA 100, 9274–9279.

11. Moretti, M., Prina-Mello, A., Reid, A. J., Barron, V. and Prendergast, P. J. (2004), ‘Endothelial cell alignment on cyclically stretched silicone surfaces’, Journal of Materials Science: Materials in Medicine 15, 1159–1164.

12. Neidlinger-Wilke, C., Grood, E. S., Wang, J. H.-C., Brand, R. A. and Claes, L. (2001), ‘Cell alignment is induced by cyclic changes in cell length: studies of cells grown in cyclically stretched substrates’, Journal of Orthopaedic Research 19, 286–293.

13. Chen, S. and Gao, H. (2006), ‘Generalized Maugis-Dugdale model of an elastic cylinder in non- lipping adhesive contact with a stretched substrate’, International Journal of Materials Research 97, 584–593.

14. Chen, S. and Gao, H. (2006), ‘Non-slipping adhesive contact between mismatched elastic spheres: A model of adhesion mediated deformation sensor’, Journal of the Mechanics and Physics of Solids 54, 1548–1567.

15. Chen, S. and Gao, H. (2006), ‘Non-slipping adhesive contact of an elastic cylinder on stretched substrates’, Proceedings of the Royal Society A 462, 211–228.

16. Chen, S. and Gao, H. (2007), ‘Non-slipping adhesive contact between mismatched elastic cylinders’, International Journal of Solids and Structures 44, 1939–1948.

17. Ghatak, A., Mahadevan, L., Chung, J. Y., Chaudhury, M. K. and Shenoy, V. (2004), ‘Peeling from a biomimetically patterned thin elastic film’, *Proceedings of the Royal Society of London, Series A* 460, 2725–2735.

18. Glass, P., Hoyong, C., Washburn, N.R., Sitti, M. (2010), ‘ Enhanced Wet Adhesion and Shear of Elastomeric Micro-Fiber Arrays with Mushroom Tip Geometry and a Photopolymerized p(DMA-co-MEA) Tip Coating.’ Langmuir 26, 17357-62.

19. Glassmaker, N. J., Jagota, A., Hui, C.-Y., Noderer, W. L. and Chaudhury, M. K. (2007), ‘Biologically inspired crack trapping for enhanced adhesion’, *Proceedings of the National Academy of Sciences USA* 104, 10786–10791.

20. Guduru, P. R. (2007), ‘Detachment of a rigid solid from an elastic wavy surface: Theory’, *Journal of the Mechanics and Physics of Solids* 55, 445–472.

21. Guduru, P. R. and Bull, C. (2007), ‘Detachment of a rigid solid from an elastic wavy surface: Experiments’, *Journal of the Mechanics and Physics of Solids* 55, 473–488.

22. Kim, S., Aksak, B. and Sitti, M. (2007), 'Enhanced adhesion of elastomer microfiber adhesives with spatulate tips', *Applied Physics Letters* 91, 221913.

23. Murphy, M.P, Kim, S, Sitti, M. (2009). 'Enhanced Adhesion by Gecko-Inspired Hierarchical Fibrillar Adhesives.' *ACS Applied Materials & Iterfaces* 1, 849-855.

24. Nadermann, N, Ning, J, Jagota, A, Hui, C.Y. (2010). 'Active Switching of Adhesion in a Film- terminated Fibrillar Structure.' *Langmuir* 26, 15464-15471.

25. Noderer, W. L., Shen, L., Vajpayee, S., Glassmaker, N. J., Jagota, A. and Hui, C.-Y. (2007), 'Enhanced adhesion and compliance of film-terminated fibrillar structures', *Proceedings of the Royal Society A* 463, 2631–2654.

26. Rand, C.J and Crosby, A.J. (2009). 'Friction of soft elastomeric wrinkled surfaces.' Journal of Applied Physics 106, 064913.

27. Hutchinson, J. W. and Suo, Z. (1992), Mixed mode cracking in layered materials, in J. W. Hutchinson and T. Y. Wu, eds, 'Advances in Applied Mechanics', Vol. 29, Academic Press, Boston, pp. 63–191.

28. J.F. Waters, P.R. Guduru. Mode-mixity-dependent adhesive contact of a sphere on a plane surface. *Proceedings of the Royal Society*, A., 466: 1303-1325 (2010).

29. J.F.Waters and P.R. Guduru. "A Mechanism for Enhanced Static Sliding Resistance due to Surface Waviness." Accepted for Publication in *The Proceedingds of the Royal Society* A. (2010).

30. Chaudhury, M. K. and Whitesides, G. M. (1991), 'Direct measurement of interfacial interactions between semispherical lenses and flat sheets of poly(dimethylsiloxane) and their chemical derivatives', Langmuir 7, 1013–1025.

31. Johnson, K. L., Kendall, K. and Roberts, A. D. R. (1971), 'Surface energy and the contact of elastic solids', Proceedings of the Royal Society of London, Series A 324, 301–313.

32. Liechti, K. M. and Chai, Y. S. (1992), 'Asymmetric shielding in interfacial fracture under in-plane shear', Journal of Applied Mechanics 59, 295–304.